

Susceptibility effects in white matter: Orientation dependence under a plurality of contrast mechanisms

Sean Foxley¹, Way Chering Chen¹, and Karla L Miller¹
¹FMRIB Centre, University of Oxford, Oxford, United Kingdom

Introduction.

Magnetic susceptibility contrast in the brain is an area of intense recent research, with a range of intriguing results in both gray and white matter. Several groups have demonstrated signal dependence on the orientation of white matter tracts with respect to B_0 . This dependence has been observed in a range of contrast mechanisms that are sensitive to susceptibility differences, including GRE phase^{1,2}, GRE magnitude^{2,3} and balanced SSFP asymmetries⁴. In the present study, we focus on signals that are sensitive to the distribution of frequencies within a voxel: GRE magnitude and BSSFP asymmetry (this differs from phase measurements which detect the mean frequency). The latter method detects asymmetries in the BSSFP frequency profile, which are driven by asymmetries in the underlying frequency distribution (as detected with the multi-GRE method). The breadth of this distribution is related to T_2^* (or more precisely, to $T_2' = (T_2^{*-1}T_2^{-1})^{-1}$), but there is also evidence that a single T_2^* value is insufficient to explain signal decay⁵, which may relate to frequency asymmetries. In this work, we compare multi-GRE- and BSSFP-based measurements for tracts with approximately parallel or perpendicular orientations, demonstrating orientation dependencies that suggests a common susceptibility effect. In another abstract, we present a model of microstructural compartmentalization that predicts many of these effects. If true, these methods may provide important microstructural biomarkers (e.g., of myelination, iron content or axonal geometry).

Methods.

Data acquisition. Multi-echo GRE and BSSFP profile measurements were obtained in five subjects on a Siemens Trio 3T with a 12-ch receive coil. GRE data was acquired at TE=4-260ms, ΔTE=2ms in five slices (2×2×2mm, 96×96 matrix, inter-slice gap 1cm, TR=1.5s, 10 averages, 25 minutes). BSSFP frequency dependence was measured across one profile band (f=0-82 Hz, Δf=1 Hz) as described previously⁵ (2×2×2mm, 110×110×30 matrix, TE/TR=6/12ms, 10° flip angle, 3s dummy cycling, 10.5 minutes). Diffusion-tensor images were acquired to extract tract orientation (2×2×2mm, whole-brain, b=1000 s/mm², 30 directions, blip-reversed acquisitions for distortion correction). Finally, a whole-brain GRE scan and T1-weighted structural were acquired for registration purposes. **Data processing.** The T_2^* was fit voxel-wise to the multi-echo GRE data at TE=4-160ms. For these TEs, white matter signal remained well above the noise floor; nevertheless, a Rician noise term was estimated from the real component at long TE and included in the fit to avoid a noise bias. The residual time course (T_2^* fit minus GRE data) was calculated to determine the deviation from mono-exponential decay (after normalization to the fit zero intercept, so that the deviation curve expresses the fractional decay that is non-exponential). The magnitude frequency spectrum for each voxel was calculated from the multi-GRE data; the asymmetry of this frequency distribution was calculated as $A_{GRE} = (L-R)/(L+R)$, where L/R is the area under the left/right half of the measured spectrum. BSSFP asymmetries, A_{BSSFP} , were calculated voxel-wise after re-centering the profile using the same asymmetry metric. **ROI analysis.** T_2^* , A_{GRE} and A_{BSSFP} values were extracted from a series of white matter ROIs. Each ROI is an intersection of a subject-specific global white-matter mask, a tract of interest in a probabilistic atlas, and a subject-specific orientation mask. Orientation masks were based on voxels with DTI estimates that are parallel ($\leq 15^\circ$ from the transverse plane) or perpendicular ($\leq 30^\circ$ from the longitudinal axis) to B_0 . In total, we considered three ROIs for parallel tracts (CST=corticospinal tract, CC=corpus callosum, SLF=superior longitudinal fasciculus) and three for perpendicular tracts (CC, OR=optic radiations, CING=cingulum bundle). Statistical analysis of measures was performed using SPSS.

Results.

Figure 1 shows the average deviation from mono-exponentiality across ROIs, with error bars indicating the between-subject standard error. Reproducible deviation appears to depend on orientation as seen by plots of ROI's perpendicular ("perp") vs. parallel ("par") to B_0 . The perpendicular tracts exhibit a characteristic ringing shape with inflection points at fairly reproducible TEs (~20, 45 and 100ms). The parallel tracts exhibit less ringing, and are dominated by a slower drift. These deviations may have the same underlying cause of BSSFP asymmetries. Average T_2^* values across ROIs computed from the fits were consistent with previously reported results, indicating 2 statistical subgroups. Although no orientation information was provided to the statistical test, these subgroups exactly group tracts by orientation (Table 1a). Similar results were found for both multi-GRE and BSSFP asymmetries, although the cingulum and parallel CC occupy something of an intermediate space (Table 1b,c), also reflected in Fig. 1.

Discussion.

Results corroborate a clear dependence of T_2^* and BSSFP asymmetry on white matter tract orientation relative to B_0 . The deviation from mono-exponentiality also exhibits orientation dependence; however, variability across ROIs with similar orientation suggests a potentially more complicated effect. This is supported by asymmetry measurements from both multi-GRE and BSSFP data; compared with T_2^* these both produce a statistical group of values consisting of both orientations. We hypothesize that micro-structural compartmentalization of susceptibility affects the frequency distribution,

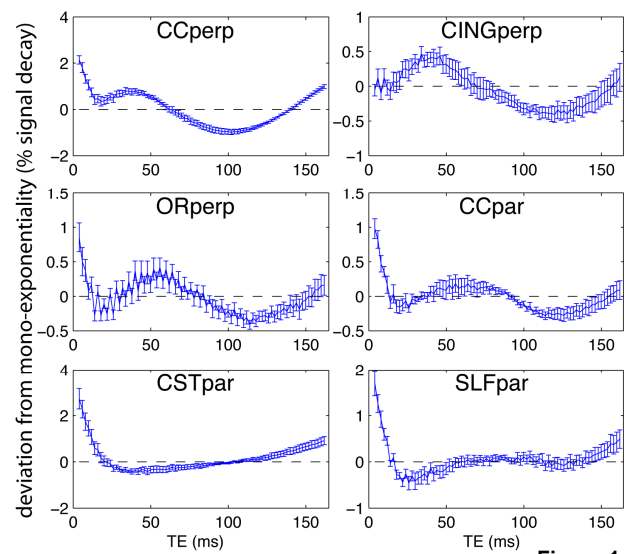


Figure 1

Table 1

ROI	(a) T_2^* (ms)		Subsets for $\alpha = 0.05$			(c) A_{BSSFP} (%)		
	1	2	1	2	3	1	2	3
OR_perp	47.8 ± 1.1		-3.0 ± 0.3			10.3 ± 1.0		
CC_perp	47.4 ± 1.2		-4.2 ± 0.3	-4.2 ± 0.3		10.4 ± 0.9		
CING_perp	48.2 ± 1.1			-5.2 ± 0.3		8.4 ± 0.3	8.4 ± 0.3	
CC_par		56.4 ± 1.1		-4.9 ± 0.2			5.6 ± 0.6	5.6 ± 0.6
CST_par		56.7 ± 2.2		-5.8 ± 0.4	-5.8 ± 0.4			4.3 ± 0.5
SLF_par		58.8 ± 1.2			-7.0 ± 0.5			4.9 ± 0.5

Statistical significance was computed using one-way analysis of variance (ANOVA) after testing normality of each sample population using a Shapiro-Wilk test. The Levene test indicated homogeneity of variance across the means, and significant homogeneous subsets of means (reported in columns) were determined with a Scheffé post hoc test.

- [1] Lee, PNAS 2010
- [2] Denk NMR Biomed 2010
- [3] Bender NMR Biomed 2010
- [4] Miller MRM 2010
- [5] van Gelderen MRM 2010